Turkish Journal of Electrical Engineering & Computer Sciences

http://journals.tubitak.gov.tr/elektrik/

Research Article

Turk J Elec Eng & Comp Sci
(2020) 28: 394 – 403

doi:10.3906/elk-1905-41

A compact wideband series linear dielectric resonator array antenna

Yazeed M QASAYMEH*, **Abdullah AlMUHASIEN**, **Talha KAMRAN**
Department of Electrical Engineering, Faculty of Engineering, Majmaah University, Saudi Arabia

Received: 08.05.2019 • **Accepted/Published Online:** 08.10.2019 • **Final Version:** 27.01.2020

Abstract: This communication presents a miniaturised series linear wideband array of notched rectangular dielectric resonator antennas that operate in the band IEEE 802.11a. Three dielectric resonators (DRs) were excited through the aperture slots coupled with a microstrip feed. To improve the array gain, the aperture slots were placed based on the attributes related to the standing-wave ratio on a short-ended microstrip feeder to obtain optimal joint power for the DRs, while the bandwidth was improved using the notched rectangular DRs. An equivalent impedance model of the proposed array was postulated to provide physical insight into the array resonance behaviour. The impedance model was simulated using the Agilent Advanced Design System software and optimised to determine the DRs' dimensions. Then the array prototype was simulated and experimentally implemented. The maximum measured gain across a 1.68-GHz bandwidth was found to be 8.28 dBi. The antenna structure measured approximately 60×40 mm, thereby making it a good component for wireless communication systems.

Key words: Antenna array, dielectric resonator antenna, gain, modelling, wideband

1. Introduction

The first dielectric resonator antenna (DRA) was introduced by Long et al. in 1983 [1]. Since then, several researchers have focused on investigating DRAs. Several advantages are ascribed to DRA, not limited to low volume, low cost, minimal loss, light weight, and convenient excitation. The single DRA designs are normally low gain but they can contribute to a broad radiation pattern. However, DRAs can be built into an array to enhance the gain. Several types of feeding techniques have been explored by researchers, such as linear array of DRAs on microstrip lines [2], slot coupled microstrip corporate feed linear DRA arrays [3], microstrip corporate feed having probe coupling DRA arrays [4], and dielectric image guide feed [5].

So far, various serial feed DRA array topologies [2] and parallel feed topologies [6] have been reported. The parallel and corporate feeds have advantages in terms of excitation networks for printed antenna arrays and exhibit design flexibility and the possibility of forming two-dimensional arrays [6]. However, these methods have some drawbacks during prototyping, including unbalanced pattern and mutual coupling effects between the elements and feed network. The series feed topology represents a more concise network, because it requires shorter transmission lengths and fewer junctions, thereby resulting in lower insertion loss.

The bandwidth of a conventional DRA is normally less than 10%, which limits its use. Hence, many researchers have attempted to improve the bandwidth of DRAs. Kishk et al. suggested the use of stacked DRAs made of multiple substances to obtain twofold resonance operations [7], and an improvement in bandwidth of up to 25% was achieved. This was followed by others who also started using stacking methods [8–10]. Various techniques have also been recommended to expand the bandwidth of DRAs, such as embedded DRAs [11,12],

*Correspondence: y.qasaymeh@mu.edu.sa

T-shaped structures [13], L-shaped structures [14], DRAs with an air space in between [15], notched DRAs [16], and combining two or more DRA modes [17,18]. Bandwidth of 30%–65% may be obtained through these methods, similar to those reported in the literature [2,19].

Very few rounded wideband DRA arrays have been mentioned in the reviewed literature. Petosa et al. reported a wideband array that implemented the small-reflections theory [2]. The determination of a configuration for the component space required a decrease in the fed reflection, thereby improving the impedance bandwidth. The bandwidth improved up to 18% and the 3 dB addition pattern bandwidth was upgraded by 17%. Zhang et al. introduced a new type of DRA for a wideband that was built with an upper resonator that was hexagon-shaped and a lower resonator that was triangle-shaped [20]. A 76.25% corresponding bandwidth was attained with the radiation pattern (broad-side), where the impedance bandwidth covered a frequency range of 5.1 to 11.1 GHz. Furthermore, Lee and Simons employed two parasitic dielectrics with one on each side of a centre DRA placed above a grounded slot coupled with a coplanar waveguide [3]. The bandwidth was increased by 3.7% using these parasitic dielectric resonator (DR) elements.

The present communication addresses a miniaturised design of a wideband DRA array operating in the 802.11ac band, considering gain enhancement. The array gain was enhanced using the characteristic concerning the proportion of the standing wave on the short-ended microstrip. The wideband resonance was obtained by introducing notched DRA elements, as a trade-off to the corresponding low Q (a mixture of air and DRA). A slot coupling feeding technique was applied to isolate the DRs from the feeding network.

2. Antenna geometry

The DRA is fed with a 50-Ω microstrip with a width of 1.4 mm on an RO4003C substrate with ε_s of 4.6 and 0.75 mm thickness. ZrSnTiSiO material with a dielectric constant $\varepsilon_r = 10$ was exploited as a resonator. Microstrip fed slot coupled antennas were first introduced in 1985 [21]. The convenient coupling with microwave integrated circuits at RF makes this technique common. It is also important to carefully choose the rectangular slot length and width to provide effective DRA coupling. However, it should not be so large as to produce vibrations in the operating frequency, which normally results in a relevant back-lobe radiation [22,23].

Figure 1 depicts the notched rectangular DRA architecture. The low permittivity rectangular DRAs can offer a bandwidth of approximately 10%. To improve the bandwidth, the notched rectangular DRA, as illustrated in Figure 1, is introduced, presenting a bandwidth amounting to 28% [16]. A notched DRA normally has a lower Q-factor in comparison with a solid rectangular DRA, where a broader bandwidth can be obtained. The Q-factor can be reduced by eliminating the fundamental slice of a rectangular DRA, because it is mixed with air permittivity ($\varepsilon_1 = 1$). The notch is adjusted in terms of its width and length, as a wideband or dual band. The dimensions were optimised for the maximisation of the bandwidth, and simultaneously maintaining the levels of low cross-polarisation. The bandwidth of the DRA can be calculated using the radiation Q-factor [24] as follows:

$$BW = \beta/Q\sqrt{\beta}, \tag{1}$$

where β denotes the maximum voltage standing wave ratio.

The concept of the short-circuited quarter-wavelength was exploited to develop the microwave-circuit application. The concept of a $\lambda/4$ stub on the short-ended feed line was implemented to maximise the coupled power in the antenna [17,23]. The stub length was calculated as follows:

$$S = \lambda_g/4, \tag{2}$$

where λ_g represents the guided wavelength.

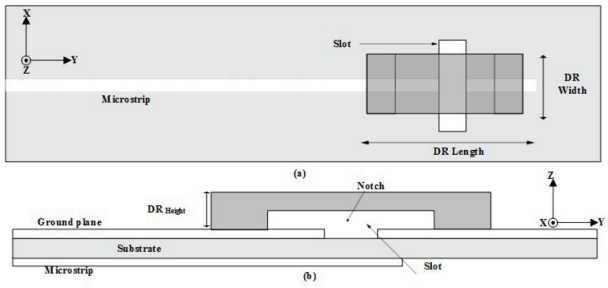

Figure 1. Architecture of the notched rectangular DRA: (a) top view and (b) side view.

The antenna structure consisted of three slots located on a ground plane and a microstrip line on the front plane, whereas the DRs were mounted above the slots. The first slot was placed $\lambda/4$ apart from the end of the microstrip. Because the antinodes repeated themselves every half-wavelength over the shorted-microstrip next to the first antinode, the remaining two coupling slots were each placed at $\lambda/2$ toward the front of the microstrip to achieve all-out coupling for maximisation of the radiation of the DRs. Figure 2 depicts the suggested array. The antenna comprises the feeder (microstrip) and the slots that couple the DRs. The DR elements that are mounted above the slots are omitted for better visualisation of the feeding technique used in coupling. The separation of elements, S_2, is equivalent to a half-wavelength, whereas the quarter-wavelength, S_1, denotes the eventual array element. The distance between the source and starting element, which is less than the half-wavelength to prevent excess antinodes above the microstrip, is represented by X.

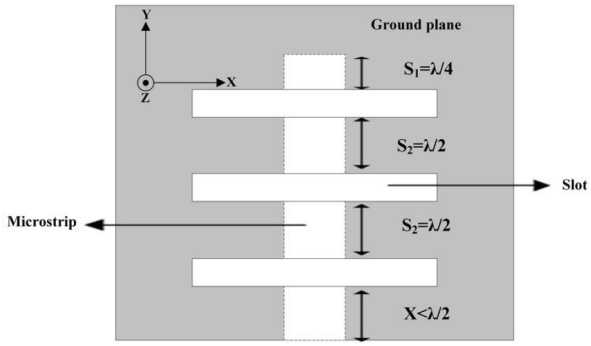

Figure 2. Suggested array demonstrating the spaces between the elements.

3. DRA-array modelling

The impedance of the proposed antenna was analysed to determine the length, width, and height of a rectangular DR, as an alternative method to the equations reported previously [22], which must be solved recursively. To achieve a wideband operation along with directive radiation, three DR array elements were assumed to be different in dimensions. An equivalent circuit model was postulated to describe and enable the quantification of individual resonant frequencies of the three DRs composing the array. Figure 3 depicts an equivalent model of a single DR antenna, fed with a coupled microstrip slot. The DRA array model comprises three resonance circuits representing three different frequencies: f_{01}, f_{02}, and f_{03}. A procedure is presented to give a physical insight into the wideband resonance of the DRA array, as illustrated previously [10,23]. The frequency resonance of the initiated DRA array suggests that the antenna supports triple resonance operations. This is evident by observing the input reflection coefficient, indicating three close valleys, which can be manipulated by changing

the dimensions of the DRs. In addition, different slot dimensions were assumed to obtain different resonant frequencies.

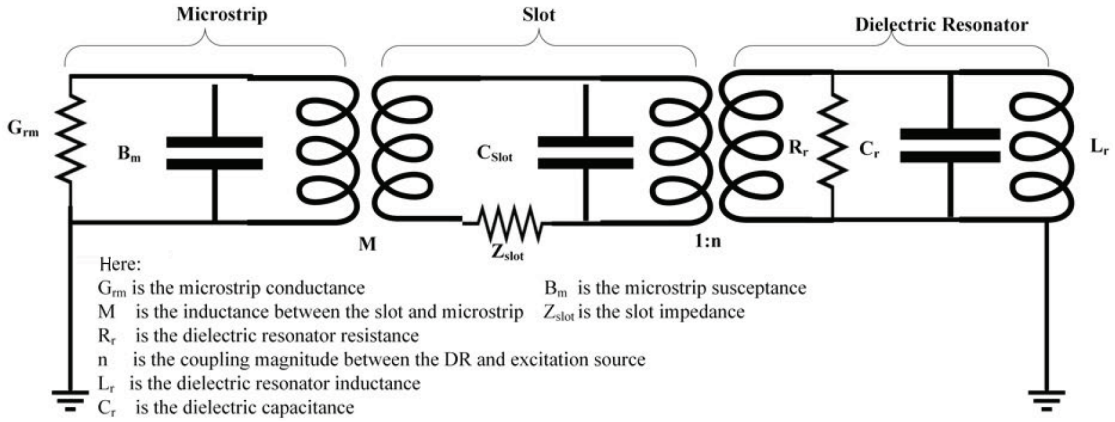

Figure 3. Microstrip slot-coupled single DR equivalent circuit model.

The equations that represent the DR as a parallel RLC model were reported before [25], once the DR was coupled with an excitation source:

$$R_r = (2n^2 z_0 S_{11})/(1 - S_{11}), C_r = (Q_0)/(\omega_0 R_r), L_r = (1)/(\omega_0 C_r), \tag{3}$$

where S_{11} denotes the reflection coefficient, z_0 is the characteristic impedance, Q_0 is the quality factor, and n is the coupling magnitude between DR and slot.

It is evident from Equation (3) that the value of R_r has a significant role in the determination of C_r and L_r. It has been reported [25] that the R_r value can be selected. For that, a complex process is required to achieve a reasonable value for R_r. To achieve this, the Agilent Advanced Design System (ADS) software is used to optimise the values of RLC. Next, MATLAB is used to determine the dimensions of DR based on the optimised RLC values. The symbol n in Equation (3) denotes the amount of coupling between the excitation source and DR (slot in this case), which plays a significant part in determining R_r, C_r, and L_r later.

The second step is to find the input impedance of the slots. Once the microstrip is terminated by a stub of length $\lambda_g/4$ (antinode), the fed impedance is calculated using the line, which is assumed to be infinitely long, and added to the series reactance, $X = -j\ Z_c\ cot(\beta_f L_t)$:

$$Z_{slot} = z_c \times (2S_{11}/S_{11} - 1) + X = z_c \times (2S_{11}/S_{11} - 1) + jZ_c cot(\beta_f L_t), \tag{4}$$

where Z_c is the characteristic transmission-line impedance [26], S_{11} is the reflection coefficient, β_f is the propagation constant, and L_t is the stub length. Z_{slot} can be measured by the program given previously [27].

The third step is to find the microstrip fed line input impedance. The input impedance at the locations of antinodes offers high resistance. As shown previously [23], the admittance as an input Y_m turns out to be equivalent to $G_{rm} + jB_m$, where G_{rm} represents the radiation conductance and B_m denotes the susceptibility of the bordering field capacitance of the microstrip. G_{rm} and B_m were reported previously [28,29], expressed by

$$G_{rm} = (160\pi^2 h^2)/(z_{cm}^2 \lambda^2 \varepsilon_{cm}) \tag{5}$$

$$B_m = \omega_0 C_l, C_l = (l_{eq} C \sqrt{\varepsilon_{cm}})/(Z_{cm}), \tag{6}$$

where h denotes the substrate height, Z_{cm} is the characteristic impedance of the microstrip, ε_{cm} is the effective dielectric constant, l_{eq} is the equivalent extra length of the microstrip, and c is the speed of light.

The last step is the transformation of the impedance that exists in the slot along the microstrip. The inductance between the slot and microstrip was reported previously [30] and represented as

$$M = (\mu_0 W_s)/(2\pi) \ln \sec(\Theta), \Theta = aractan(L_s/2h), \tag{7}$$

where W_s is the slot width, L_s the slot length, h is the substrate height, and μ_0 is the free space permeability.

Every antenna impedance function has an equivalent circuit in Darlington form. The dimensions of the slots were assumed, and their relative impedances were calculated using Equation (4). The impedances of 50 microstrips were calculated from Equations (5) and (6). The three-stage circuit, as shown in Figure 3, was built in Agilent ADS, which represents the array including the uncalculated values of parallel RLCs, representing the three DRs. Using Agilent ADS, the three parallel RLCs were tuned to resonate at the desired frequency, and then a MATLAB program based on Equation (3) was used to extract the dimensions of each DR according to its resonant frequency. No wideband operation was expected in this stage, because the model does not include the mutual coupling between the DRs. Once the input impedance model is successful, the antenna will be modelled in computer simulation technology (CST). The measurements for return loss, radiation pattern, and gain, compared with the results obtained from CST, will be the final step in the design.

4. Outcomes with discussion

Three DRA array elements were modelled in the corresponding impedance circuit using Agilent ADS. Diverse measurements of length and width in the slots were presumed for varying quantities of coupling to attain a wideband operation. The impedance that exists between the microstrip, slot, and coupling can be calculated using Equations (5)–(7), as illustrated in Section 3. Because the impedances of the slot and microstrip are static, the parallel RLC network that represents the DR can be adjusted by Agilent ADS, thereby enabling the antenna to strike resonance at three distinct resonant frequencies. As mentioned in Equation (3) and explicated in Section 3, the value of R_r is significant in determining C_r and L_r. Thus, R_r was set to be 55 to obtain the values of rational C_r and L_r. Next the optimised R_r, L_r, and C_r values were put into MATLAB to derive the dimensions of DRs, by solving Equation (3). Figure 4 depicts the impedance model of the proposed three-element DRA array. Figure 5 demonstrates the dimensions of the suggested array elements. During the calculating and modelling of the DRs, they were assumed to be rectangular without a notch in the centre, because the notch size is smaller in comparison with the size of the DR. The same height of 0.5 mm was applied to every notch in each DR. By solving Equation (2), at a frequency of 5.8 GHz, the $\lambda/4$ wavelength S_1 and $\lambda/2$ wavelength S_2 were found to be 7.9 and 15.8 mm, respectively, whereas the value of X was set to be 10 mm to prevent further antinodes on the feeder.

Figure 6 depicts the simulated power antinodes on the microstrip executed with the CST software. The figure shows how the antinodes take their positions at the locations obtained from Equation (2) at 5.8 GHz. The DRs were mounted above the coupling slots placed over the antinodes.

Figure 7 shows the return-loss results through simulation and measurement. Three resonant frequencies were obtained by Agilent ADS at 5.15, 5.39, and 5.74 GHz, which represent the operating frequencies of the three single DRs. The simulated CST bandwidth was between 5.04 and 5.95 GHz, with minimal return loss of –22 dB at 5.8 GHz with an impedance of 45.23–j5.33 Ω. The measured bandwidth ranges from 5.25 to 5.91 GHz, with minimum return loss at 5.635 GHz of –25.116 dB and impedance of 48.55–j2.23 Ω. The consistency between

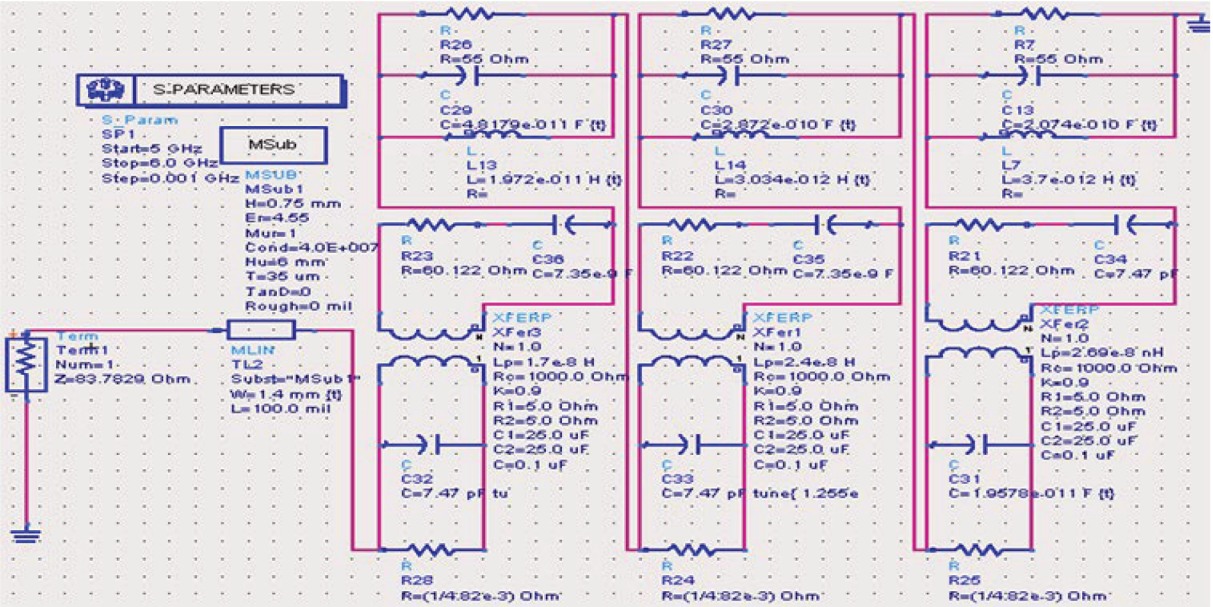

Figure 4. Impedance model of the dielectric resonator array in Agilent ADS.

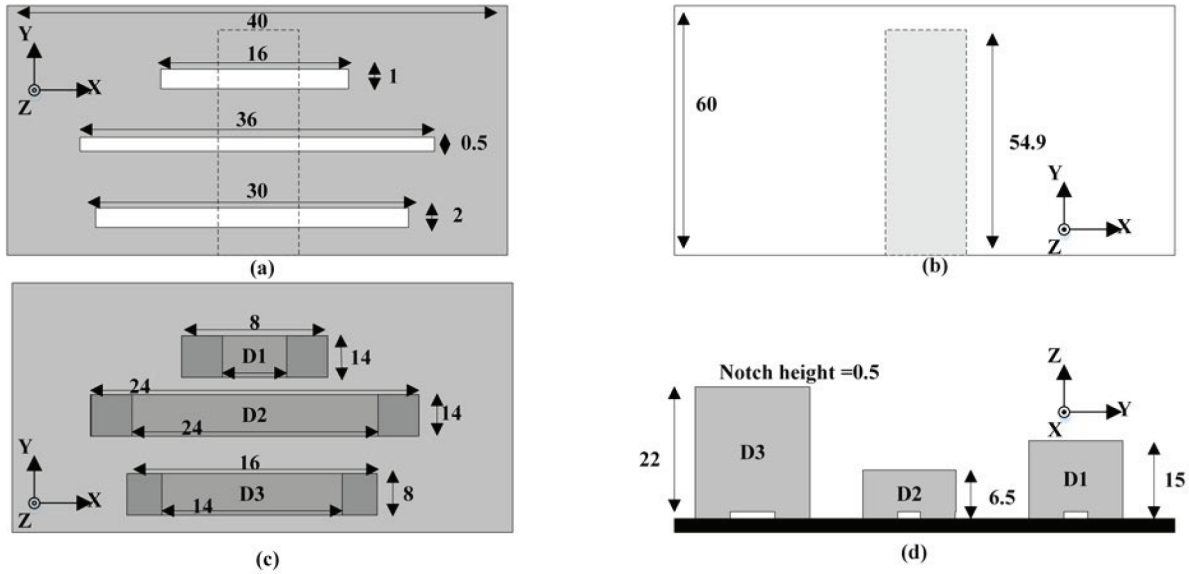

Figure 5. Designed structure in CST: a) slots' dimensions, b) microstrip dimensions (width = 1.7mm), and c and d) dielectric elements' dimensions (all dimensions in mm).

the simulated and measured results is reasonable. The discrepancies are related to the minute fabrication error, and the nonuniformity was caused by the manual soldering of SMA connectors. The microwave vector network analyser model HP 8720D was used to execute the measurement.

Figure 8 depicts the antenna gain in the frequency between 5.1 and 5.9 GHz. The maximum simulated gain of 8.4 dBi occurs at 5.9 GHz, which was derived from the CST software through simulation. The maximum measured gain occurs at 5.9 GHz of 8.28 dBi, using the gain transfer method that compares the antenna to a standard known gain monopole antenna. This indicates that the gain of the proposed DRA array was of enhanced efficiency. During the measurements, a reflector can be used to enhance the gain up to 12.2 dBi. The

signal generator model number HP83620B and spectrum analyser model number Agilent 8565E were used to perform the measurement of the gain at different frequencies.

Figure 9 depicts the measured and simulated radiation patterns in the direction of the xz and yz plane at 5.8 GHz. For the xz plane simulation radiation pattern, the main loop magnitude was 8.4 dBi, whereas the measurement was 8.28 dBi for the same direction. For the radiation in the yz plane, the maximum simulated magnitude was 3.3 dBi and maximum measured was 2.8 dBi. The agreement between the simulated and measured results was fairly good. A reflector can be used to reduce the back loop radiation from the feeder side and to focus the radiation more towards the DR elements. The signal generator model number HP83620B and spectrum analyser model number Agilent 8565E were used for the measurement setup to measure the radiation pattern at 5.8 GHz.

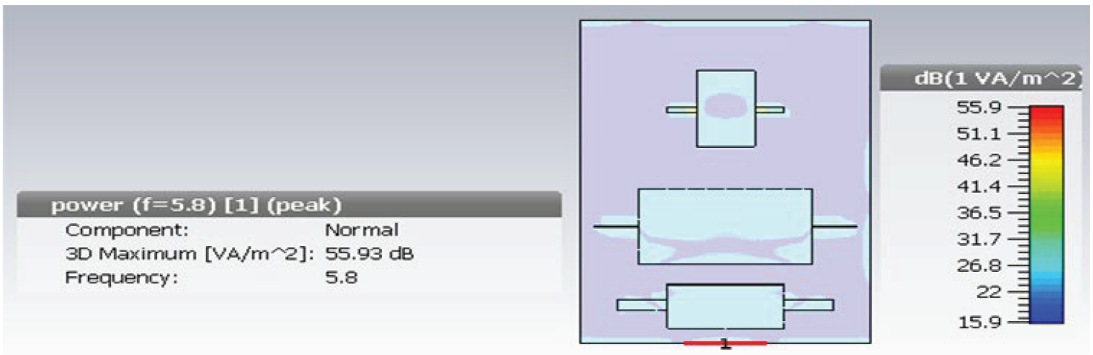

Figure 6. 5.8 GHz radiation power antinodes over the microstrip simulated using CST.

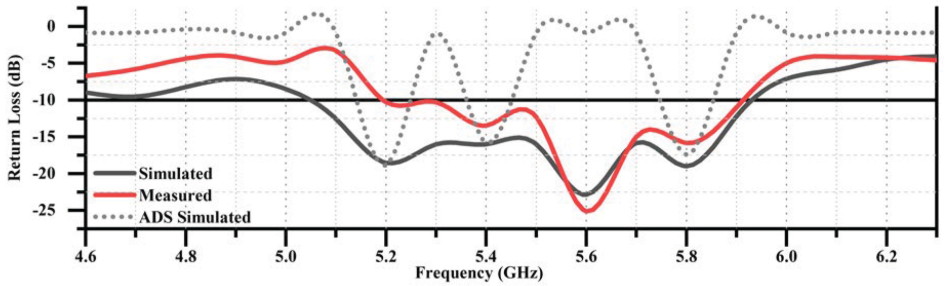

Figure 7. Measured and simulated return loss.

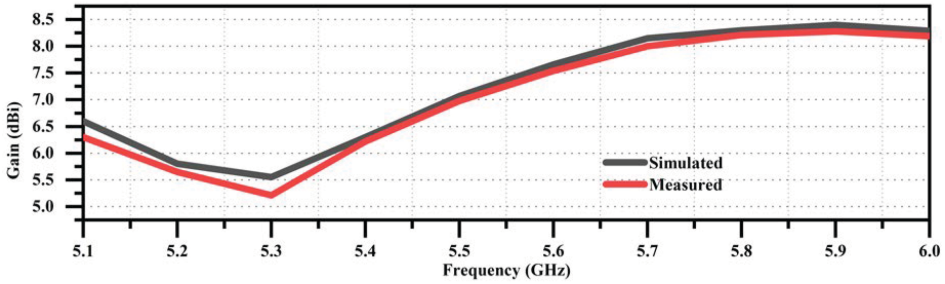

Figure 8. Measured and simulated gains of the antenna.

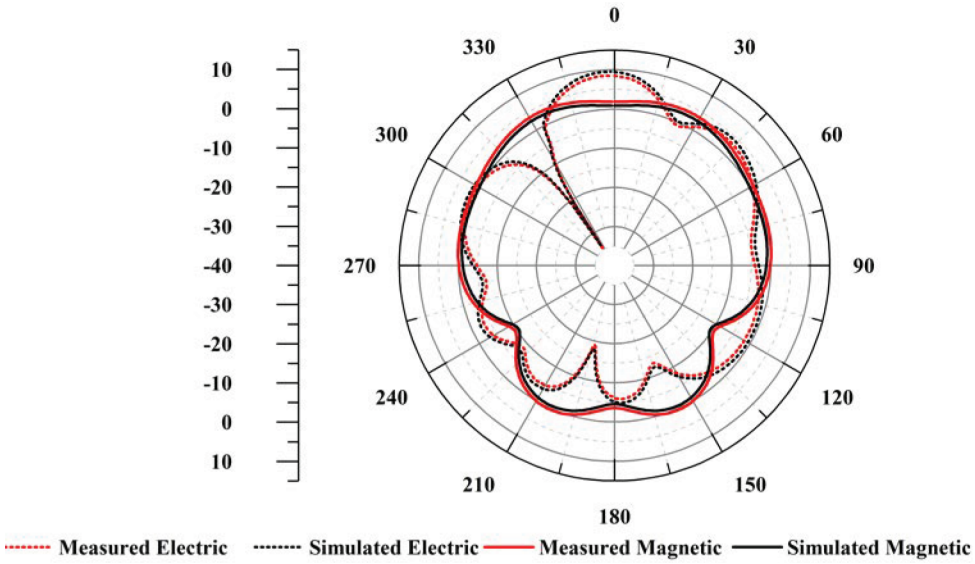

Figure 9. Measured and simulated 5.8 GHz radiation patterns of the DRA in the xz and yz planes.

Table 1. Comparison of the work conducted in the present paper with serially fed wideband DRA arrays reported in the literature.

Published work	Wideband technique	Frequency band	Gain	Array size [length, width, height]
Petosa et al. (1996) [2]	Paired DRAs depending on small theory reflections	6.34 to 7.6 GHz 23.03%	14.1 dBi	$7.04\lambda_0 \times 5.59\lambda_0 \times 0.00054\lambda_0$
Lin et al. (2017) [31]	Rectangular rings mounted on DRs	6.72 to 9.88 GHz 38.1%	15.7 dBi	$6.24\lambda_0 \times 1.037\lambda_0 \times 0.0127\lambda_0$
Nikkhah et al. (2013) [32]	Adding slots array below the DRA elements	8.8–9.6 GHz 4.3%	20 dBi	$16.56\lambda_0 \times 1.073\lambda_0 \times 0.023\lambda_0$
Proposed work	Notched DRA	5.25–5.91 GHz 59.13%	8.28 dBi	$1.159\lambda_0 \times 0.773\lambda_0 \times 0.0145\lambda_0$

5. Conclusion

A three-element DRA array with a compact size of $60 \times 40mm$ was presented in this study. A larger bandwidth ranging from 5.25 to 5.91 GHz was obtained with a notable gain enhancement. A microstrip slot coupled structure fed the postulated arrays employing the attribute of the short-ended microstrip line. The array comprising the suggested notched DRA increased the gain and impedance bandwidth responses, thereby making the array potentially useful in IEEE 802.11a band communication channels. Table 1 shows a comparison between several reported series linearly fed DRA arrays and the array presented in the present report. Table 1 shows a notable size reduction and a wider resonance impedance compared with those documented in the literature.

Acknowledgement

The authors would like to thank the deanship of scientific research at Majmaah University for supporting this work under project number 56-1439. The authors thank the anonymous reviewers for their constructive comments.

References

[1] Long S, McAllister M, Shen L. The resonant cylindrical dielectric cavity antenna. IEEE Transactions on Antennas and Propagation 1983; 25 (3): 406-412. doi: 10.1109/TAP.1983.1143080

[2] Petosa A, Ittipiboon A, Cuhaci M, Larose R. Bandwidth improvement for a microstrip-fed series array of dielectric resonator antennas. Electronics Letters 1996; 32 (7): 608-609. doi: 10.1049/el:19960451

[3] Lee R, Simons R. Bandwidth enhancement of dielectric resonator antennas. Proceedings of IEEE Antennas and Propagation Society International Symposium; Ann Arbor, MI, USA; 1993, pp. 1500-1503.

[4] Eshrah I, Kishk A, Yakovlev A, Glisson A. Theory and implementation of dielectric resonator antenna excited by a waveguide slot. IEEE Transactions on Antennas and Propagation 2005; 53 (1): 483-494. doi: 10.1109/TAP.2004.838782

[5] Al-Zoubi A, Kishk A, Glisson A. Analysis and design of a rectangular dielectric resonator antenna fed by dielectric image line through narrow slots. Progress in Electromagnetics Research 2007; 77: 379-390. doi: 10.2528/PIER07082504

[6] Petosa A, Larose R, Ittipiboon A, Cuhaci M. Microstrip-fed array of multisegment dielectric resonator antennas. IEE Proceedings - Microwaves, Antennas and Propagation 1997; 144 (6): 472-476. doi: 10.1049/ip-map:19971375

[7] Kishk A, Ahn B, Kajfez B. Broadband stacked dielectric resonator antennas. Electronics Letters 1989; 25 (18): 1232-1233. doi: 10.1049/el:19890826

[8] Antar Y, Fan Z. Theoretical investigation of aperture-coupled rectangular dielectric resonator antenna. IEE Proceedings - Microwaves, Antennas and Propagation 1996; 143 (2): 113-118. doi: 10.1049/ip-map:19960269

[9] Shum S, Luk K. Stacked annular-ring dielectric resonator antenna excited by axi-symmetric coaxial probe. IEEE Transactions on Antennas and Propagation 1995; 43 (8): 889-892. doi: 10.1109/8.402212

[10] Coulibaly Y, Denidni TA, Talbi L. Wideband impedance bandwidth hybrid dielectric resonator antenna for X-band applications. IIEEE Antennas and Propagation Society International Symposium; Albuquerque, NM, USA; 2006. pp. 2429-2432.

[11] Walsh A, DeYong C, Long S. An investigation of stacked and embedded cylindrical dielectric resonator antennas. IEEE Antennas and Wireless Propagation Letters 2006; 5: 130-133. doi: 10.1109/LAWP.2006

[12] Kishk A. Experimental study of broadband embedded dielectric resonator antennas excited by a narrow slot. IEEE Antennas and Wireless Propagation Letters 2005; 4: 79-81. doi: 10.1109/LAWP.2005.844648

[13] Rao Q, Denidni T, Sebak A. Broadband compact stacked T-shaped DRA with equilateral-triangle cross sections. IEEE Microwave and Wireless Components Letters 2006; 16 (1): 7-9. doi: 10.1109/LMWC.2005.861360

[14] Denidni T, Rao Q, Sebak A. Broadband L-shaped dielectric resonator antenna. IEEE Antennas and Wireless Propagation Letters 2005; 4: 453-454. doi: 10.1109/LAWP.2005.860198

[15] Junker G, Kishk A, Glisson A, Kajfez D. Effect of air gap on cylindrical dielectric resonator antenna operating in TM01 mode. Electronics Letters 1994; 30 (2): 97-98. DOI: 10.1049/el:19940114

[16] Ittipiboon A, Cuhaci M, Mongia R, Bhartia P, Antar Y. Aperture fed rectangular and triangular dielectric resonators for use as magnetic dipole antennas. Electronics Letters 1993; 29 (23): 2001-2002. doi: 10.1109/TAP.1986.1143929

[17] Ittipiboon A. An investigation of a novel broadband dielectric resonator antenna. IEEE Antennas and Propagation Society International Symposium; Baltimore, MD, USA; 1996. pp. 2038-2041.

[18] Almpanis G, Fumeaux C, Vahldieck R. The trapezoidal dielectric resonator antenna. IEEE Transactions on Antennas and Propagation 2008; 56 (9): 2810-2816. doi: 10.1109/TAP.2008.928787

[19] Kishk A, Yin Y, Glisson A. Conical dielectric resonator antennas for wideband applications. IEEE Transactions on Antennas and Propagation 2002; 50 (4): 569-474. doi: 10.1109/TAP.2002.1003382

[20] Zhang X, Lai Q, Ma X. Novel hexagon shaped dielectric resonator antenna array for wideband applications. 3rd IEEE International Symposium on Microwave, Antenna, Propagation and EMC Technologies for Wireless Communication; Beijing, China; 1985. pp. 639-642.

[21] Pozar D. Microstrip antenna aperture-coupled to a microstripline. Electronics Letters 1985; 21 (2): 49-50. doi: 10.1049/el:19850034

[22] Pozar D. A reciprocity method of analysis for printed slot and slot-coupled microstrip antennas. IEEE Transactions on Antennas and Propagation 1986; 34 (12): 1439-1446. doi: 10.1109/TAP.1986.1143785

[23] Sullivan P, Schaubert D. Analysis of an aperture coupled microstrip antenna. IEEE Transactions on Antennas and Propagation 1986; 34 (8): 977-984. doi: 10.1109/TAP.1986.1143929

[24] Mongia R, Bhartia P. Dielectric resonator antennas — a review and general design relations for resonant frequency and bandwidth. International Journal of RF and Microwave Computer-Aided Engineering 1994; 4 (3): 230-247. doi: 10.1002/mmce.4570040304

[25] Collin E. Foundations for Microwave Engineering. New York, NY, USA: McGraw-Hill, 1992.

[26] Junker G, Kishk A, Glisson A. Input impedance of aperture-coupled dielectric resonator antennas. IEEE Transactions on Antennas and Propagation 1996; 44 (5): 600. doi: 10.1109/8.496245

[27] Mirshekar-Syahkal D. Spectral Domain Method for Microwave Integrated Circuits. New York, NY, USA: Wiley, 1990.

[28] Akhavan H, Mirshekar-Syahkal D. Approximate model for microstrip fed slot antennas. IEEE Electronics Letters 1994; 30 (23): 600. doi: 10.1049/el:19941300

[29] Akhavan H, Mirshekar-Syahkal D. A simple technique for evaluation of input impedance of microstrip-fed slot antennas. Ninth International Conference on Antennas and Propagation, ICAP '95; Eindhoven, Netherlands; 1995. pp. 265-268.

[30] James J, Henderson A. High-frequency behaviour of microstrip open-circuit terminations. Microwaves, Optics and Acoustics 1979; 3 (5): 205-218. doi: 10.1049/ij-moa.1979.0046

[31] Lin J, Shen W, Yang K. A low-sidelobe and wideband series-fed linear dielectric resonator antenna array. Antennas and Wireless Propagation Letters 2017; 16: 513-516. doi: 10.1109/LAWP.2016.2586579

[32] Nikkhah M, Mohassel J, Kishk A. A low sidelobe and wideband series-fed dielectric resonator antenna array. 21st Iranian Conference on Electrical Engineering (ICEE); Mashhad, Iran; 2013. pp. 1-3.